Br Cy

WRDC-TR-90-4023
ADA221886

COMPRESSIVE STRENGTH OF RIGID-ROD POLYMER FIBERS

Charles Y-C. Lee
Polymer Branch
Nonmetallic Materials Division

U. Santhosh
AdTech Systems Research
1342 N. Fairfield Road
Dayton, OH 45432

March 1990

Interim Report for Period April 1989 - December 1989

Approved for Public Release; Distribution Unlimited

MATERIALS LABORATORY
WRIGHT RESEARCH AND DEVELOPMENT CENTER
AIR FORCE SYSTEMS COMMAND
WRIGHT-PATTERSON AIR FORCE BASE, OHIO 45433-6533

NOTICE

When Government drawings, specifications, or other data are used for any purpose other than in connection with a definitely Government-related procurement, the United States Government incurs no responsibility or any obligation whatsoever. The fact that the government may have formulated or in any way supplied the said drawings, specifications, or other data, is not to be regarded by implication, or otherwise in any manner construed, as licensing the holder, or any other person or corporation; or as conveying any rights or permission to manufacture, use, or sell any patented invention that may in any way be related thereto.

This report is releasable to the National Technical Information Service (NTIS). At NTIS, it will be available to the general public, including foreign nations.

This technical report has been reviewed and is approved for publication.

R. C. Evers
Polymer Branch
Nonmetallic Materials Division

T. E. HELMINIAK, Chief
Polymer Branch
Nonmetallic Materials Division

FOR THE COMMANDER

MERRILL L. MINGES, Director
Nonmetallic Materials Division

If your address has changed, if you wish to be removed from our mailing list, or if the addressee is no longer employed by your organization please notify WRDC/MLBP, WPAFB, OH 45433-6533 to help us maintain a current mailing list.

Copies of this report should not be returned unless return is required by security considerations, contractual obligations, or notice on a specific document.

REPORT DOCUMENTATION PAGE

Form Approved
OMB No. 0704-0188

1a. REPORT SECURITY CLASSIFICATION Unclassified	1b. RESTRICTIVE MARKINGS
2a. SECURITY CLASSIFICATION AUTHORITY	3. DISTRIBUTION/AVAILABILITY OF REPORT Approved for public release; distribution unlimited
2b. DECLASSIFICATION/DOWNGRADING SCHEDULE	
4. PERFORMING ORGANIZATION REPORT NUMBER(S) WRDC-TR-90-4023	5. MONITORING ORGANIZATION REPORT NUMBER(S)
6a. NAME OF PERFORMING ORGANIZATION Materials Lab, WRDC, AFSC 6b. OFFICE SYMBOL (If applicable) WRDC/MLBP	7a. NAME OF MONITORING ORGANIZATION
6c. ADDRESS (City, State, and ZIP Code) Wright-Patterson Air Force Base, OH 45433-6533	7b. ADDRESS (City, State, and ZIP Code)
8a. NAME OF FUNDING/SPONSORING ORGANIZATION same as 6a 8b. OFFICE SYMBOL (If applicable)	9. PROCUREMENT INSTRUMENT IDENTIFICATION NUMBER
8c. ADDRESS (City, State, and ZIP Code)	10. SOURCE OF FUNDING NUMBERS PROGRAM ELEMENT NO. 61102F; PROJECT NO. 2303; TASK NO. Q3; WORK UNIT ACCESSION NO. 07

11. TITLE (Include Security Classification)
Compressive Strength of Rigid-Rod Polymer Fibers

12. PERSONAL AUTHOR(S)
Charles Y-C Lee and U. Santhosh

13a. TYPE OF REPORT	13b. TIME COVERED	14. DATE OF REPORT (Year, Month, Day)	15. PAGE COUNT
Interim	FROM Apr 89 TO Dec 89	1990 March 1	52

16. SUPPLEMENTARY NOTATION

17. COSATI CODES			18. SUBJECT TERMS (Continue on reverse if necessary and identify by block number)
FIELD	GROUP	SUB-GROUP	
07	04		
11	04		

19. ABSTRACT (Continue on reverse if necessary and identify by block number)
Various mechanical models describing the buckling of a single column and a bundle of columns were reviewed. The relationship between these models and the buckling of a polymeric fiber with substructures (fibril, microfibril, and individual chain) were discussed. It was found that the structural element that has the lowest critical buckling strength will initiate the compressive failure of the fiber. The critical strength is dependent on the element geometry and the strength of the interaction with the neighbors. In previous analysis in the literature, the equations were applied to the molecular chain level. This study shows that the analysis is more appropriate at the fibril level (diameter of 0.1μm). This can account for the failure of many attempts in improving the compressive strength by modifying the molecular structure. The fiber torsion test was reassessed and some preliminary cold draw experiments were reported.

20. DISTRIBUTION/AVAILABILITY OF ABSTRACT ☒ UNCLASSIFIED/UNLIMITED ☐ SAME AS RPT. ☐ DTIC USERS	21. ABSTRACT SECURITY CLASSIFICATION Unclassified
22a. NAME OF RESPONSIBLE INDIVIDUAL Charles Y-C Lee	22b. TELEPHONE (Include Area Code) 513-255-9155 22c. OFFICE SYMBOL WRDC/MLBP

DD Form 1473, JUN 86 *Previous editions are obsolete.*

TABLE OF CONTENTS

LIST OF FIGURES

LIST OF TABLES

FOREWORD

This report was prepared by the Polymer Branch, Nonmetallic Materials Division. The work was initiated under Project No 2303, "Nonmetallic and Composite Materials," Task No. 2303Q3, Work Unit Directive 2303Q307, "Structural Resin." It was administered under the direction of Materials Laboratory, Wright Research and Development Center, Air Force Systems Command, Wright-Patterson Air Force Base, Ohio, with Dr R. C. Evers as the Materials Laboratory Project Scientist. Co-authors were Charles Lee, Materials Laboratory (WRDC/ MLBP) and U. Santhosh (Adtech Systems Research). This report covers research conducted from April 1989 to December 1989.

SECTION I
INTRODUCTION

The high modulus of advanced polymeric fibers along with its low density makes them an attractive choice of material in many weight sensitive aerospace structural applications. The specific stiffness and tensile strength of high performance polymeric fibers like poly (p-phenylene terephthalamide) or PPTA, commercially sold as Kevlar, and poly (p-phenylene benzobisthiazole) or PBT, make them much superior to conventional materials like steel and aluminium. Among the currently available polymers poly (p-phenylene benzobisoxazole) or PBO and PBT have the best thermal stability and the highest stiffness and strength [1]. These properties combined with their excellent radiation resistivity and environmental resistance give them a wide scope of application in aircraft and space structures. However their current application in reinforced structures like composites is limited by their poor compressive strength. Unlike metals and alloys which these polymers propose to replace and which have compressive strengths comparable to or superior to their tensile strengths, polymeric fibers have relatively low compressive strengths, usually less than 10% of their tensile strengths.

The high specific stiffness and strength of polymeric fibers like PPTA, PBO and PBT are obtained by using a rigid chain molecular architecture and by ensuring the extension of the polymer chains either by drawing during the fiber extrusion process or during subsequent heat treatment. It has been well documented in the literature [2-4] that these fibers have a fibrillar morphology with a wide range of dimensions for the fibril diameters. Due to their slender geometry all these structural units will tend to buckle under a compressive load. The different possible modes of buckling of the fibrillar fiber can be categorized into two depending on whether the entire fiber buckles as a homogeneous structural unit or whether the fibrils constituting the fiber buckle in unison.

Numerical results from these models applied at the chain level in the fiber morphology have been given in reference [5]. The results indicate a fiber compressive strength equal to the shear modulus of the fiber. These models are re-examined in sections II and III. In section IV the results of the above models have been viewed at the different levels of the fiber morphology to see how it affects the overall compressive strength of the fiber. The scope of considering alternate molecular architectures in order to improve the fiber compressive strengths are also discussed along with some work done in this area.

Torsional oscillation of fibers are used in literature [6] to yield their shear modulus which is related to the shear mode buckling strength in fibrillar fibers. The axial tension applied to the fiber during the measurement affects the value of the measured shear modulus. Section V reviews the mechanics of the torsion of an axially loaded fiber using the incremental deformation theory and re-interprets the experimental data in terms of the interfibril sliding shear modulus in such fibers.

Finally section VI presents some preliminary results on the compressive strengths of PBO and PBT fibers in the as-spun and the heat treated states. The objective of the study is to see if the increase in the degree of extension and orientation of the fibrils and the consequent decrease in the degree of the lateral interaction that accompany the drawing process in cold draw and heat treatment have any affect on the compressive strength of the fibers.

SECTION II
BUCKLING MODELS FOR RIGID-ROD POLYMERIC FIBERS

It has been confirmed extensively in the literature that rigid rod polymeric fibers like PPTA and PBT have a fibrillar microstructure formed during coagulation [2-4]. Buckling of these fibrillar units resulting from the buckling of the entire fiber has also been observed [2, 3, 7]. The mathematical models used to determine the theoretical compressive strength of polymeric fibers due to buckling can be broadly divided into two groups: (1) that which attribute the failure of the fiber to the collective buckling of the groups of the chains or fibrils that constitute the fiber and (2) that which considers the compression of the entire fiber as a single structural unit. The various models, their assumptions and limitations and their comparison with experimental data are given below.

2.1 SINGLE FIBER BUCKLING MODELS

2.1.1 Euler Buckling

Buckling is an internal instability in slender structures caused by the decrease of their bending rigidity under the action of a compressive stress. The simplest model for the buckling of a single homogeneous fiber is that of the Euler buckling of the elastic structure (figure-1). The critical buckling load for this case is given by

$$P^E = \frac{\pi^2 E_l I}{l^2} m^2 \qquad (1)$$

Here E_l is the longitudinal modulus of the fiber, l and I are the length and the cross-sectional moment of inertia respectively of the fiber and m is the buckling mode, i.e. the number of half sine waves in the buckled shape. This expression becomes minimum when m=1 and so the critical stress for a cylindrical fiber of diameter d can be written as

$$\sigma_{cr}^E = \frac{\pi^2 E_l d^2}{16 l^2} \qquad (2)$$

2.1.2 Euler Buckling with Shear Effects

In Euler buckling it is assumed that the fiber does not experience any shear deformation. However due to the relatively low ratio of the shear to the axial modulus of polymeric fibers [8], the cross-section of the fiber undergoes significant amount of shear during deformation and this

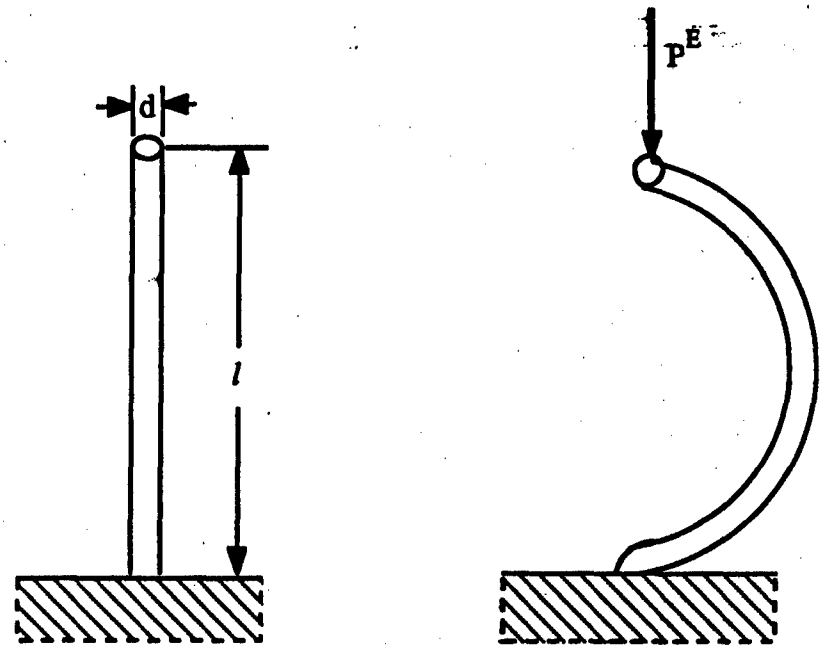

Figure-1: Column or Euler Buckling

lowers the critical buckling load. The expression for the elastic buckling load with shear for a slender column can be derived to be (pg. 132 of reference [9])

$$\sigma_{cr} = \frac{\sigma_{cr}^{E}}{1 + n\frac{\sigma_{cr}^{E}}{G}} \tag{3}$$

where G is the shear modulus of the material of the column and n is a geometric factor (equal to 1.11 for a circular cross-section and 1.20 for a rectangular cross-section).

2.1.3 Inelastic Buckling

In the above models the implicit assumption is that the fiber remains perfectly elastic till it fails. Though initially the fiber may behave in an elastic manner, it is more likely that it becomes plastic before it fails. Evidence of the kink bands in aramid filaments as being due to plastic instability has been reported in reference [10]. For a cylindrical column the critical load for the inelastic buckling can be derived to be (pg. 175 of reference [9])

$$\sigma_{cr} = \frac{\pi^2 E_T d^2}{16 l^2} \tag{4}$$

where I is the moment of inertia of the cross-section of the beam and E_T is the tangent modulus in the plastic region of the stress-strain curve at a stress equal to σ_{cr} (figure-2). This equation can be used to find the critical buckling stress from the stress-strain curve using an iterative method. For Kevlar-49 fibers, using the compressive stress-strain curve (figure-3) given in reference [11], the critical stress for inelastic buckling can be determined to be in the range of 0.36 GPa to 0.44 GPa (52 KSI to 64 KSI). This compares well with the composite test data of 0.45 GPa. However the validity of equation (4) to predict the compressive strength can only be proved by applying it to other rigid-rod polymer fibers and by direct morphological evidence of the plastic nature of the failure. Compressive stress-strain curves for other fibers well into the plastic region too have to be experimentally determined.

2.1.4 Experimental Comparison

Table-2 compares the above mentioned three Euler buckling models with experimental results for Kevlar, PBT and PBO fibers with properties given in table-1. Some of the transverse properties of PBT and PBO have been estimated taking into account their morphological similarity with Kevlar [5]. The aspect ratios used in table-2 are the ratios of the length of the fiber used in the recoil test (25.4 mm) to their diameters. It can be seen that for these fibers the stress needed to buckle them is very low. Since the observed compressive strength is much higher than the theoretical buckling strength of the fiber it can be inferred that the actual failure

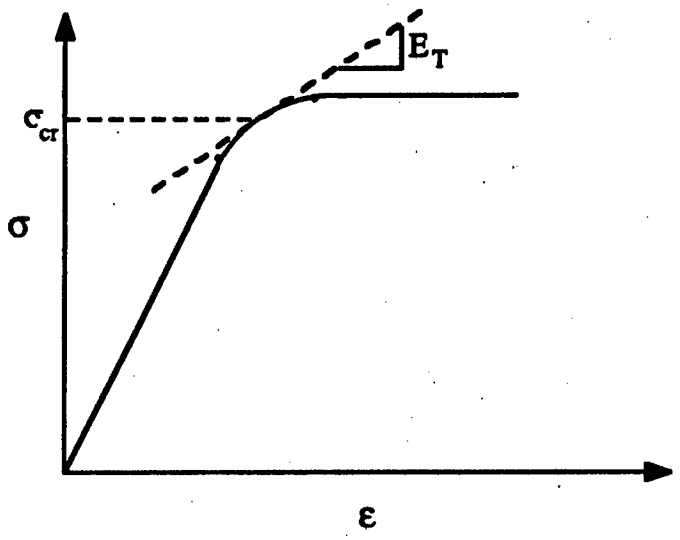

Figure-2: Buckling out of the Elastic Zone

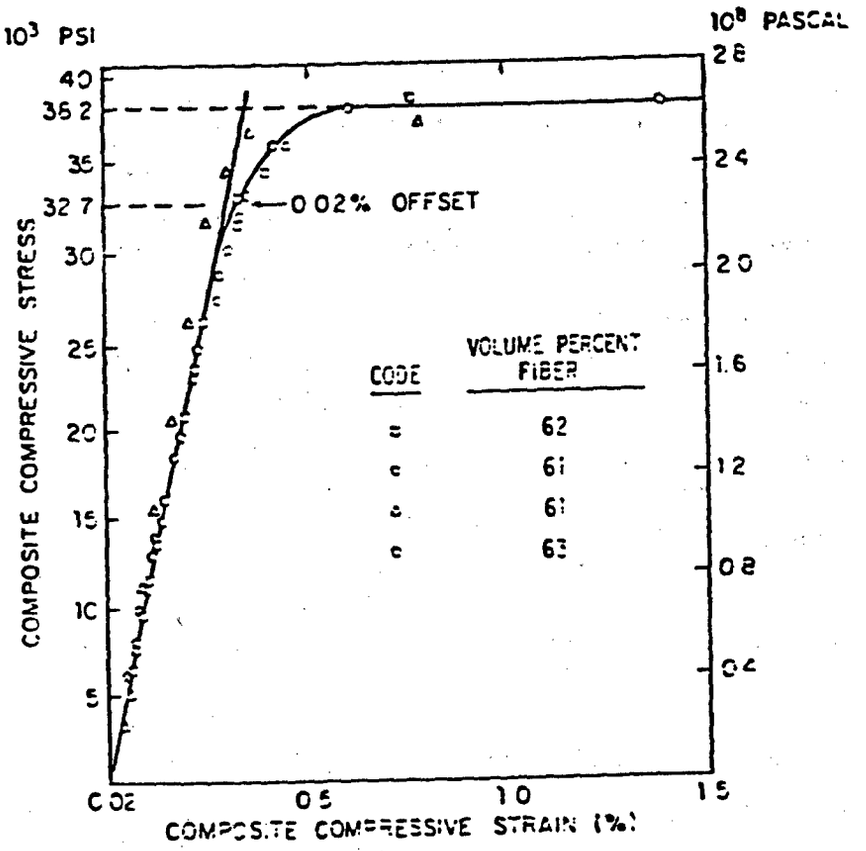

Figure-3: Compressive Stress-Strain Curve for Kevlar 49/Epoxy Unidirectional Composite [11]

Table-1: Mechanical Properties of Fibers

Fiber	Longitudinal Modulus, E_l (GPa)	Transverse Modulus, E_t (GPa)	Shear Modulus, G (GPa)
PPTA	123	0.77	1.5
PBT	265	0.5*	1.2
PBO	164	0.5*	0.6*

* Estimate

Table-2: Critical Fiber Buckling Stress (MPa)

Fiber	*l*/ D	Euler Mode (Eq. 2)	Euler Mode with Shear (Eq. 3)	Inelastic Buckling (Eq. 4)	Experimental (x 10^{-3})
PPTA	630	0.19	0.19	0.36-0.44	0.37† (0.45)*
PBT	630	0.41	0.41		0.28† (0.31)*
PBO	250	1.62	1.61		0.27

† Recoil Test Data

* Composite Test Data

during the testing is not caused by the buckling of the entire fiber. In the composite test it may be due to the fact that the Euler mode may be adequately removed due to the matrix support.

2.2 FIBRILLAR / CHAIN BUCKLING MODELS

In this description of buckling it is assumed that the fibrils or the rigid-rod chains that comprise the polymeric fibers buckle in a group. It is also assumed that these slender columns (fibrils or chains) each with a longitudinal modulus E_l, length l, diameter d, and cross-sectional moment of inertia I interact with one another. The interaction is modelled by assuming that the columns are supported by an elastic foundation with (transverse) modulus E_t and shear modulus G (figure-4). In reality these two properties quantify the combined transverse stiffness of the columns and any possible intercolumn interaction (eg. Van der Waal interaction or interfacial adhesion forces).

A system of parallel fibrils or chains described above can buckle in either of two modes, extensional mode or shear mode [5], depending on the nature of the deformation of the material between the microstructures. These modes which are similar to the buckling failure of unidirectional composites [12,13] have been discussed in detail in reference [5] and are reproduced here.

2.2.1 Extensional Mode of Buckling

In the extensional mode the adjoining columns buckle out of phase (figure-4a) and the material in between the columns undergoes extension. The buckling load can be determined by minimizing the expression for the total potential energy of a column on an elastic support [9] to be given by

$$P^e = \frac{\pi^2 E_l I}{l^2} m^2 + \frac{4E_t l^2}{\pi^2}\frac{1}{m^2} \quad \text{where } m = 1,2,3,\ldots \tag{5}$$

To determine the first buckling mode, we have to determine the value of m for which P^e is a minimum. It can be seen that in the absence of the elastic support, i.e., when E_t=0, the above equation reduces to the case of Euler buckling of each individual column and P^e is minimum for m=1. But as the non-zero value of E_t increases P^e will become minimum for progressively larger values of m. It can be shown mathematically that equation (5) becomes minimum when

$$\frac{L}{m} = \pi\sqrt[4]{\frac{E_l I}{4E_t}}$$

and the minimum value is

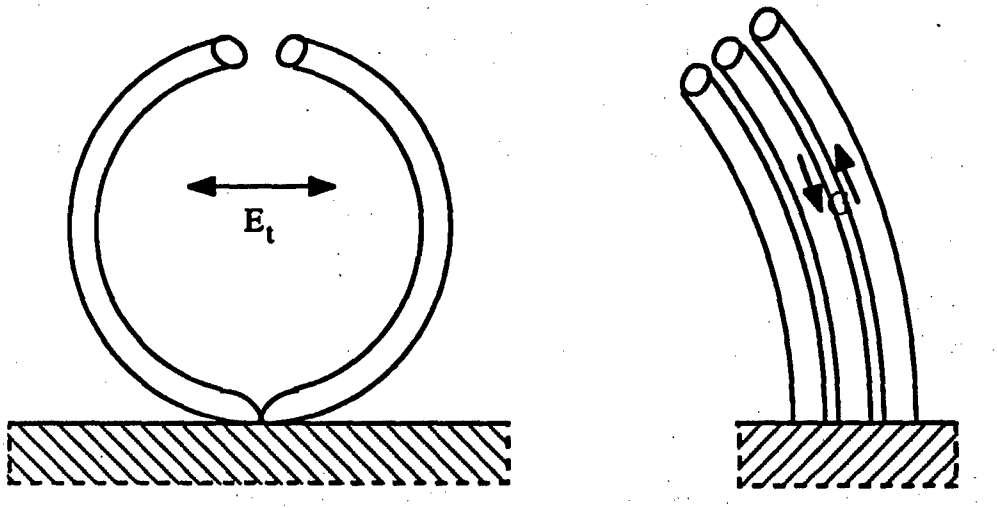

(a) Symmetric or Extensional Mode

(b) Antisymmetric or Shear Mode

Figure-4: Buckling of a Collection of Fibrils

$$P^e_{cr} = 4\sqrt{E_l E_t I} \tag{6}$$

For a cylindrical column the critical buckling stress thus becomes

$$\sigma^e_{cr} = 2\sqrt{\frac{E_l E_t}{\pi}} \tag{7}$$

The above expression has also been derived at the chain level for a rigid rod polymer in reference [5]. If E_t and k are the transverse modulus and the covalent bond bending constant of the chain the critical buckling stress has been shown to be given by

$$\sigma^e_{cr} = \frac{4\sqrt{E_t k l'}}{A} \tag{7a}$$

where l' and A are the bond length and the effective cross-sectional area of a single chain in the lattice.

2.2.2 Shear Mode of Buckling

The columns deform in phase in the shear mode of buckling causing the intermediate media to shear (figure-4b). Using the energy method [5,9] the load needed to buckle in the mth mode can be derived to be

$$P^s = \frac{\pi^2 E_l I}{l^2} m^2 + GA \qquad \text{where } m = 1,2,3,\ldots \tag{8}$$

where $A \approx d^2$ is the area. This expression becomes minimum for m=1 and so the critical load for shear mode of buckling of a cylindrical column of diameter d is

$$\sigma^s_{cr} = \frac{\pi^3 E_l}{64}\left(\frac{d}{l}\right)^2 + G \tag{9}$$

For long columns due to their very high aspect ratio (l/d) the Euler term in the above expression was considered very small compared to the second term and was neglected [5]. Therefore

$$\sigma^s_{cr} = G \tag{9a}$$

This approximation is valid at the chain level because the aspect ratio of the molecular chain is high. However, for the relatively small aspect ratios at the fibrillar level the Euler term in the equation for the shear mode buckling stress, equation (5), cannot be neglected. This is illustrated in figure-5 where the ratio of the compressive strength as given by equation-9 to the shear modulus is plotted against the aspect ratio of the buckling unit. It can clearly be seen that in the range of the fibrils, l/d < 100, the approximation of the entire shear mode buckling stress by the shear modulus is incorrect, especially for small values of the stiffness.

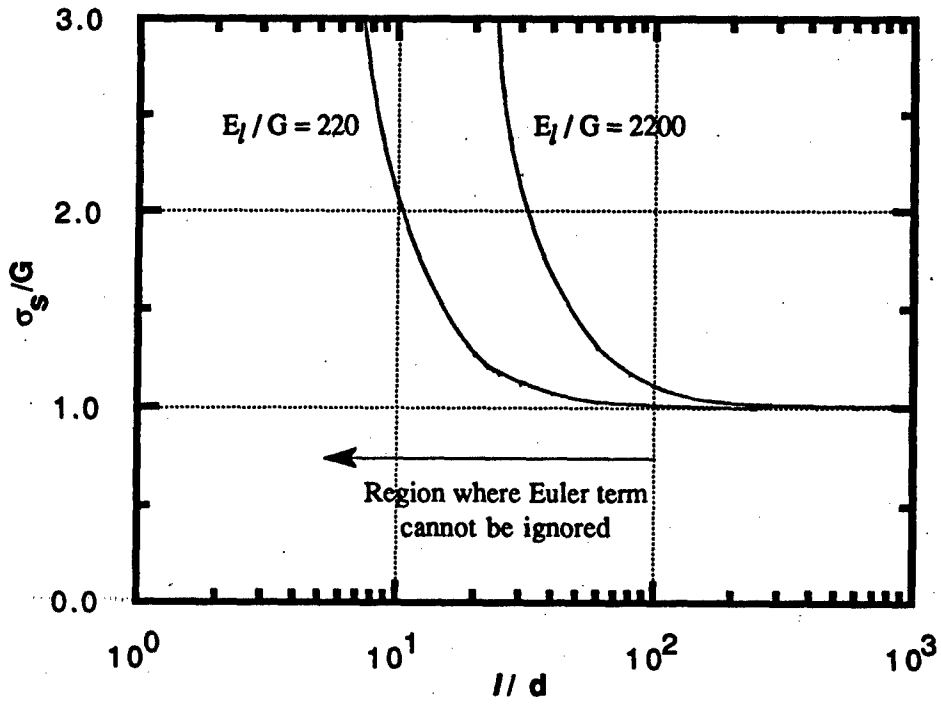

Figure-5: Influence of the Euler Term on the Shear Mode Buckling Strength

SECTION III
FIBER BUCKLING VS. FIBRILLAR BUCKLING

The different buckling models have been described above. For a transversely isotropic, homogeneous fiber that remains elastic to failure, it is obvious that equation (1) is the appropriate equation describing its buckling behavior. If the fiber is composed of fibrils, or closely packed rigid-rod molecular chains then equations (6) and (8) will describe the buckling loads of the fibrils or chains. The actual mode in which the fiber fails will then depend on which of the equations for the above mentioned three buckling loads for the fiber as a whole is a minimum.

3.1 BUCKLING EQUATIONS OF A RIGID-ROD POLYMER FIBER

Let's consider a single isotropic, homogeneous fiber. The Euler buckling load is identical to that of equation (1). The equation is rewritten here with capital letters to denote the description of the cylindrical fiber.

$$P_c = \frac{\pi^3 E_l D^4}{64L^2} \tag{1a}$$

Let's imagine that this fiber can be split into finer structures (figure-6), e.g. fibrils or molecular chains, without loss of volume. The buckling load of the bundle of N fibrils will be then

$$P_c = N\, p_c = \frac{\pi D^2}{4d^2}\, p_c \tag{10}$$

where p_c is the critical buckling load of each individual sub-element and d is the diameter of the sub-elements. If the splitting is perfect G and E_t in equations (5) and (8) can be considered as zero and then p_c will be given by

$$p_c = \frac{\pi^3 E_l d^4}{64L^2} \tag{11}$$

and the critical buckling load for the whole bundle is given by equation (1a). Next let's imagine that repair can be made to this bundle with an adhesive, again, without any change in the total volume. G and E_t are then virtually a measure of the effectiveness of the adhesive in repairing the bundle. If perfect repair can be made such that the resultant fiber possesses mechanical properties indistinguishable from the original fiber, the buckling load should again be described by equation (1a). Otherwise, the extensional and shear modes described by equations (6) and (8) respectively are two additional possible buckling modes for the fiber. Thus a complete description of the buckling of a fiber with a structure as depicted in figure-6 should be the following set of equations describing the three possible buckling modes.

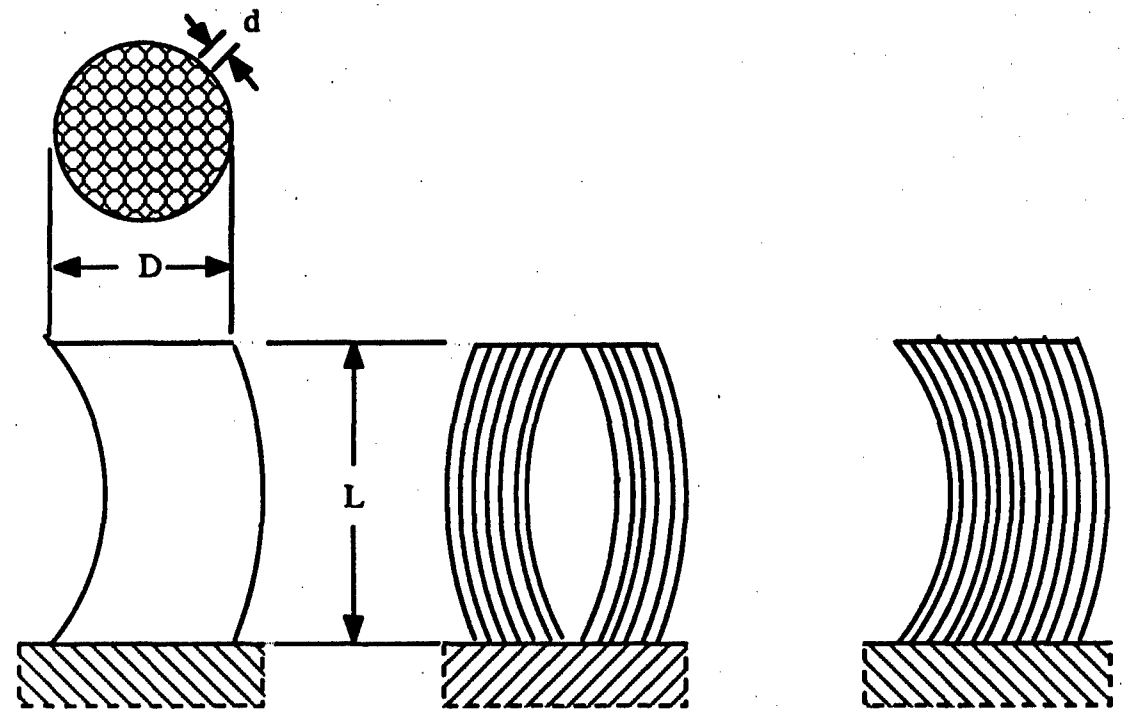

Figure-6: Buckling Modes of a Fiber with a Microfibrillar Morphology

$$P_c = \frac{\pi^3 E_l D^4}{64L^2} \tag{1a}$$

$$P_c = \frac{\sqrt{\pi^3}}{8} \sqrt{E_l E_t}\, D^2 \tag{6a}$$

$$P_c = \frac{\pi^4 E_l X^2 D^4}{256L^2} + \frac{\pi G D^2}{4} \qquad , X = \frac{d}{D} \tag{8a}$$

This is a simplified description of the possible modes; mixed modes with combinations of shear and extensional buckling are ignored. The stresses corresponding to these equations ($\sigma_c = 4P_c/\pi D^2$) are plotted in figure-7 using the elastic constants for PBT fiber [5]. The fiber will buckle according to one of the modes depicted in figure-6 depending on which of the equations (1a), (6a) or (8a) yields the lowest critical load value.

3.2 FIBER COMPRESSIVE STRENGTH AND THE BUCKLING MODES

Comparing equations (1a) and (6a) it can be shown that if

$$E_t > \frac{\pi^3}{64} \left(\frac{D}{L}\right)^4 E_l \tag{12}$$

the entire fiber will buckle as a column instead of the failure being through the extensional buckling of the fibril. Similarly if

$$G > \frac{\pi^2}{16} \left(\frac{D}{L}\right)^2 E_l \tag{13}$$

then the shear buckling of the fibril will not take place. Since D/L is usually less than one, it is obvious that G and E_t do not have to be the same order of magnitude as E_l for the fiber to buckle as a column. This exercise clearly points out that having a fibrillar structure does not necessarily mean that fibril buckling has to be the mode of failure: if the interaction between the fibrils can be sufficiently strong to satisfy equations (12) and (13), the fiber will buckle as a single element. Finally equations (6a) and (8a) yield the following third condition on whether extensional or shear mode of buckling will occur. Thus if

$$G > \frac{\sqrt{\pi}}{2} \sqrt{E_l E_t} - \frac{\pi^3 X^2}{64} \left(\frac{D}{L}\right)^2 E_l \tag{14}$$

the fiber will fail in the extensional mode.

The relationship between the fibrillar density of the fiber (D/d), the aspect ratio of the fibrils (L/d) and the different buckling failure modes can be better illustrated by rearranging the above inequalities in the following non-dimensional form after substituting for X.

$$\frac{L}{d} > \sqrt[4]{\frac{\pi^3}{64}\frac{1}{k}} \left(\frac{D}{d}\right) \tag{12a}$$

$$\frac{L}{d} > \frac{\pi}{4} \sqrt{\frac{1}{k'}} \left(\frac{D}{d}\right) \tag{13a}$$

$$\frac{L}{d} < \frac{\pi}{8} \sqrt{\frac{2\pi}{\sqrt{\pi k} - 2k'}} \tag{14a}$$

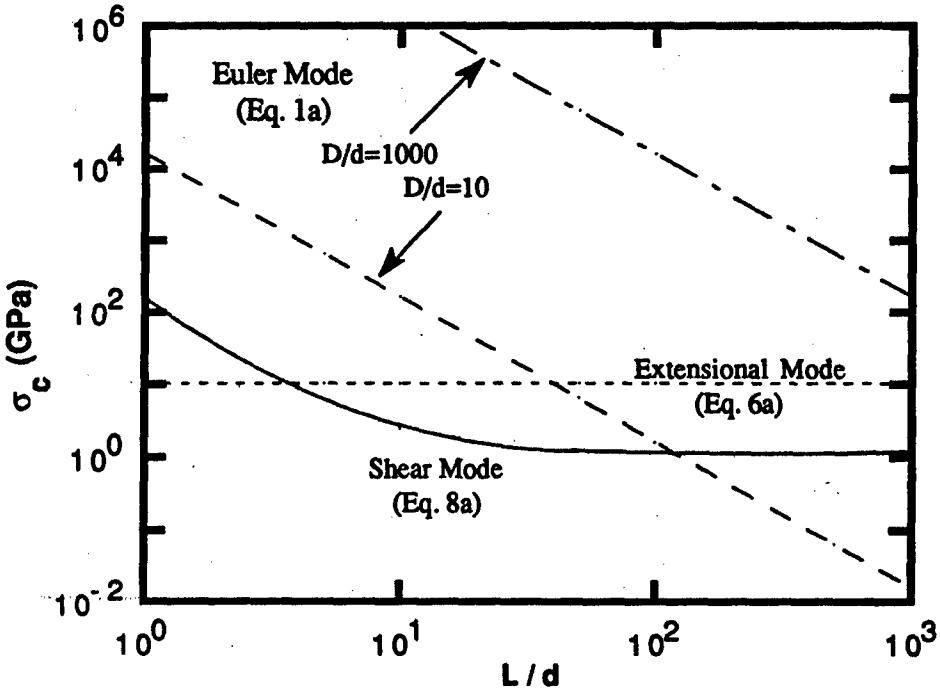

Figure-7: Fiber Buckling Stress for the Different Modes
(E_l=265GPa, E_t=0.5GPa, G=1.2GPa)

Here $k=E_t/E_l$ and $k'=G/E_l$. When these equations are plotted, as in figure-8, they identify three distinct regions --- regions where the critical buckling load for each of the three respective buckling modes is a minimum. Thus when equations (12a) and (13a) are satisfied the Euler buckling of the entire fiber dominates over the microstructural failure, while extensional mode failure of the fibrils is most dominant when equation (14a) is satisfied. At all other regions on the graph the shear buckling of the microstructure dominates the fiber failure. The critical aspect ratio of the fibril that distinguishes between the shear and extensional mode of failure, equation (14a), is independent of the fibrillar density, D/d. Instead it depends only on the relative magnitudes of E_t and G.

Figure-8(a) has been plotted for PBT fiber using the values of the transverse modulus E_t (0.5 GPa) and the sliding shear modulus G (1.2 GPa) given in reference [5]. For a fiber and fibril combination with a known geometry changing the values of G and E_t will also change the failure mode of fiber as shown in the example in figure-8(b) where E_t=0.1 GPa and G=6.0 GPa is used. Thus for a fiber in which the fibrils are such that L/d=10 to 100 and D/d=100 in the first case (figure-8(a)) the fiber is predicted to buckle in the shear mode while in the latter case (figure-8(b)) the failure is predicted to be in the extensional mode. It can also be seen that for larger size microstructures (small D/d) as the aspect ratio L/d increases the change of the buckling mode in figure-8(a) is from the extensional mode through shear to the single column mode. In figure-8(b) on the other hand the failure mode changes directly from the extensional mode to the column mode.

The differences between the buckling modes as depicted in figures-6(a) and 6(c) should be further clarified. Observing the fiber buckles macroscopically, there is no apparent difference between the two modes. However, the deformation of the volume elements in the fibril are different. In the single column buckling mode, all volume elements deform in a manner without shear deformation of the interfaces of the elements (figure-9(a)). On the other hand in the shear mode of fibrillar buckling, the volume elements in each substructure deform by the shearing of the interface between them (figure-9(b)). The length of the buckling element, L, is usually determined by the stationary points of the column under compression loading. In the Euler buckling of a single, unsupported fiber, L should be considered as the gage length of the fiber between the experimental fixture. In the consideration of the fibrillar structures in a polymeric fiber as depicted in reference [2], L should be the fibrillar length between junctions. Furthermore, the effective L may not be related to any observable morphological features of the undamaged fiber. If G and E_t are not uniform along the length of the fibrils, the effective L can be the section that has a weaker interaction with the neighbors.

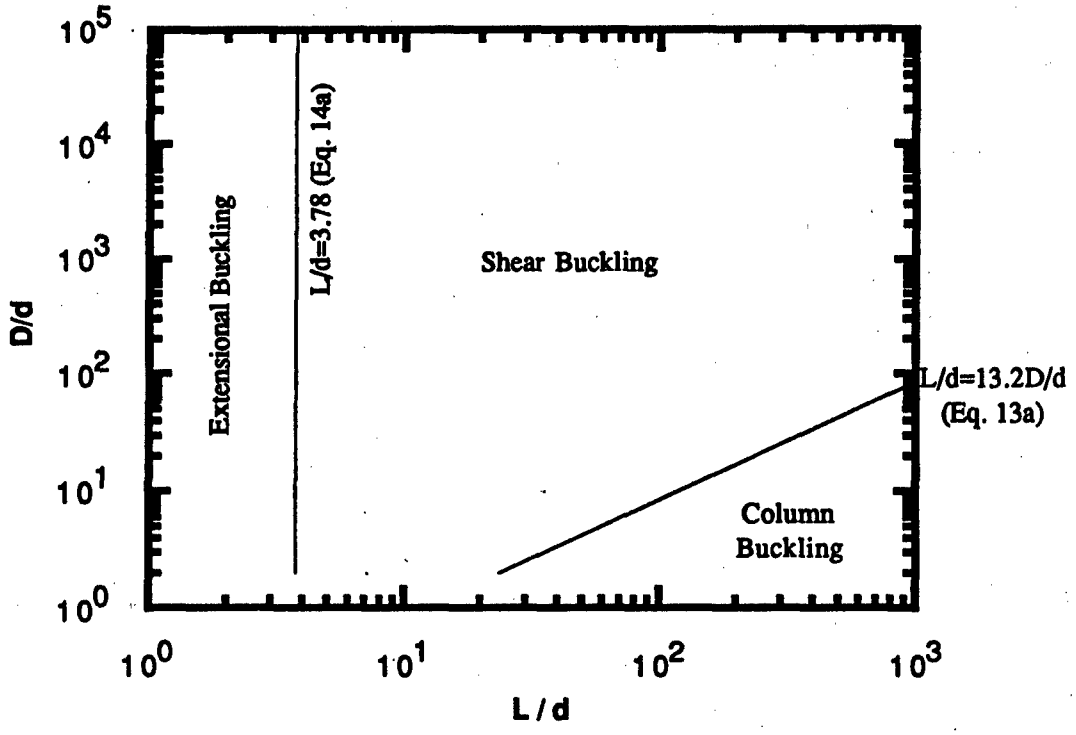

Figure-8(a): E_l=265GPa, E_t=0.5GPa, G=1.2GPa

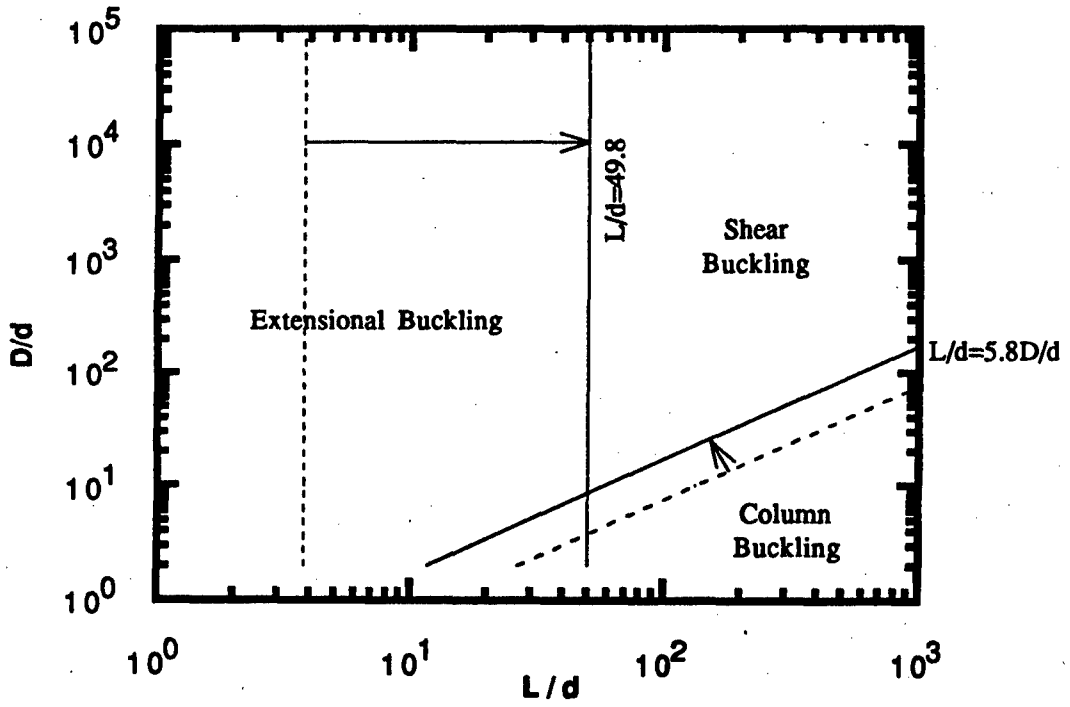

Figure-8(b): E_l=265GPa, E_t=0.1GPa, G=6.0GPa

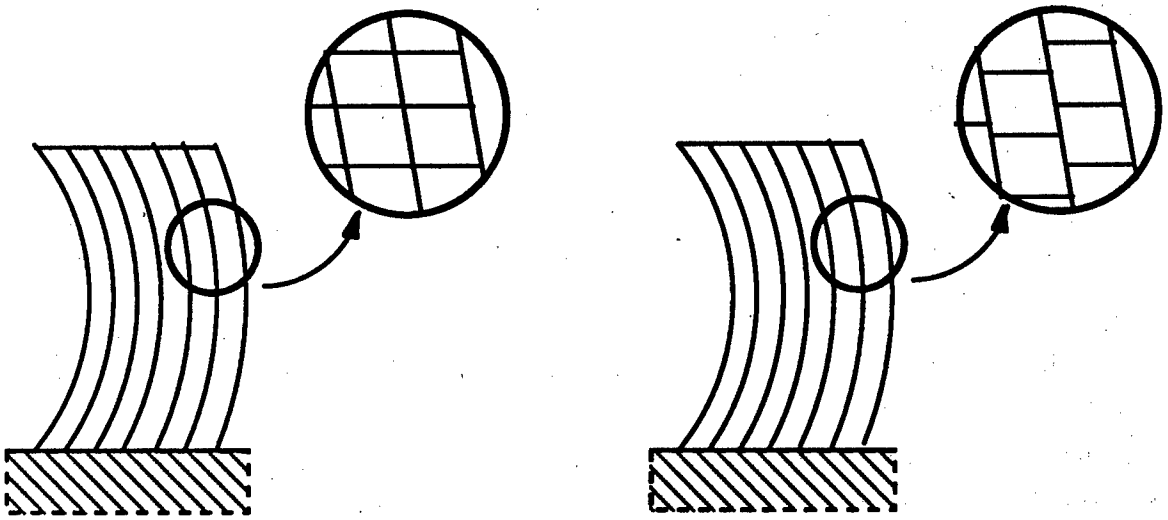

(a) Single Column Mode (b) Shear Mode

Figure-9: Deformation of Volume Elements

SECTION IV
FIBRILLAR MORPHOLOGY VS. BUCKLING STRENGTH

The fibrillar morphology of rigid-rod polymers has been well documented in literature. Cohen and Thomas [3] reported the diameter of the smallest fibrillar unit in PBT to be about 80-100 Å. At the other end of the scale 0.20-0.75 μm fibrils have been observed in mechanically peeled PBT fibers [2]. Study of SEM micrographs of PBT and other polymeric fibers show the existence of fibrils of varying diameters in the above range (table-3). Similarly the lengths of the fibrils vary over a wide range depending on the scale of the fibrillar unit being studied. Cohen and Thomas [3] determined the fibrillar length to be of the order of 10^2 to 10^3 Å, while the distance between kink bands in peeled PBT in reference [2] is about 5-20 μm. Since buckling could be initiated in any of these morphological structures the aspect ratio of the buckling unit could vary from about 500 at the chain level (assuming PBT chains of 5Å diameter and 2400Å length [5]) to a lower number at the fibrillar level.

From figure-10 it can be seen that the shear mode of failure is the most probable failure mode for all these different morphological structures having the aspect ratios mentioned above. The shear modulus used to determine the shear mode buckling in equation (8a) is that which measures the relative sliding between the fibrils. The longitudinal (or torsional) shear modulus of the fiber was used instead in references [5] and [6]. Furthermore, in equation (8a) for the small values of the sliding shear modulus G, as explained earlier in figure-5, the contribution of the Euler term may not be small enough to be neglected especially at the fibrillar level with aspect ratios less than 100.

If the fiber is not a homogeneous isotropic column each sub-fiber element (from the fibril down to individual molecular chains) will have its own set of buckling equations (1a), (6a) and (8a). Among the various dimensional substructure elements the actual unit where buckling is initiated will then be the one for which the expression for the buckling load is a minimum. This means that improving the longitudinal modulus E_l by better aligning the rigid-rod chains will not necessarily improve the compressive strength [1] as predicted by equation (2).

4.1 BUCKLING STRENGTH AND EXPERIMENTAL FIBER PROPERTIES

The material properties used in all of the above calculations have been determined experimentally by testing single filaments. The standard tensile test is used to determine the longitudinal modulus, E_l [14]. The transverse modulus of the fiber, E_t, is determined by

Table-3: Dimensional Range of Substructure Elements in a Fiber

Substructure		Dimensional Range of Diameter
Fiber		10-50μm
Fibril	Macrofibril : Microfibril	0.5μm : 2nm
Chain		Å

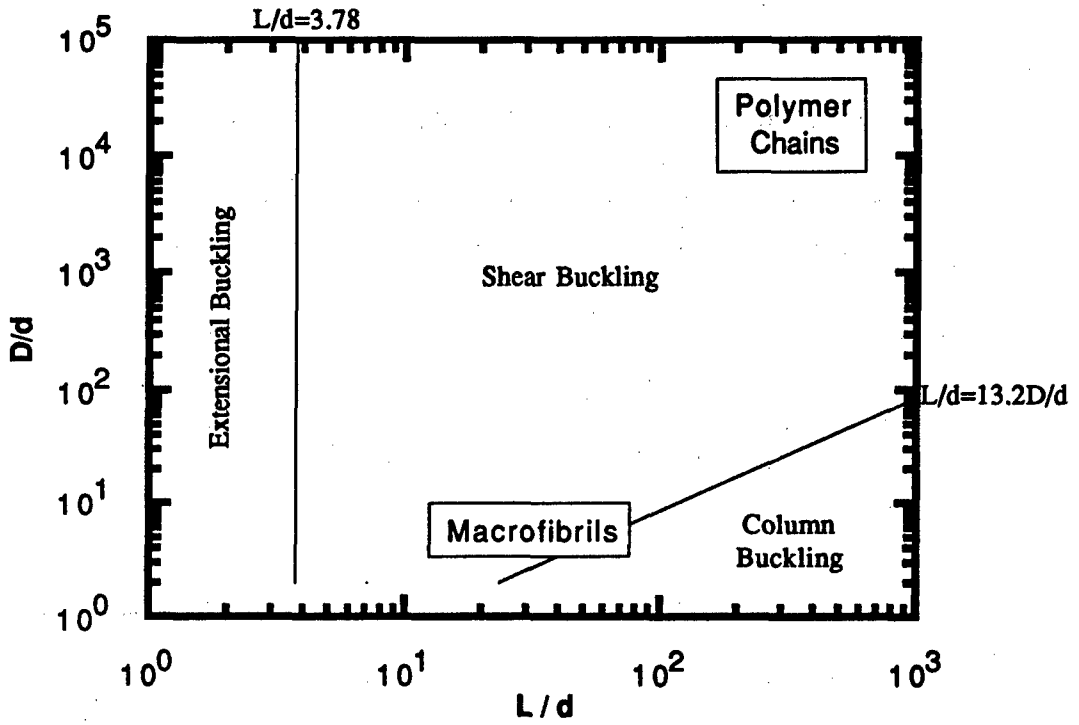

Figure-10: Relationship Between Buckling Modes and Microfibrillar Structure in PBT Fiber (E_l=265GPa, E_t=0.5GPa, G=1.2GPa)

compressing it between flat platens and simultaneously recording the platen displacement and the contact force [15,16]. Finally the oscillations of a torsional pendulum made with the filament [17, 18] is used to yield the torsional modulus of the fiber. This last measurement is discussed further in section-V. The test methods described above all determine the bulk properties of the fiber. These properties are a measure of the material of the fiber along with the defects in its microstructure and not that of the defect-free molecules or chains. In the forementioned buckling equations it is therefore more appropriate to use these material properties at the fibrillar level rather than at the chain level as done in reference [5].

As mentioned earlier the buckling of the fibrils the dominated by the weakest buckling unit, i.e., among the hierarchy of the fibrillar structure the actual fibrils where failure will initiate will have the lowest buckling load in one of the three modes -- Euler, shear or extensional. Measurement of the mechanical properties by testing individual fibers yields the average properties of the entire fiber, and does not reflect the heterogeneous fibrillar structure inside it. At the level of the individual fibrils the local mechanical properties may be quite different and lower than the measured values. For example presence of a longitudinal void between microfibrils will remove the transverse support between them, thus drastically reducing the local transverse modulus. As explained through figures 8(a) and (b) in section III, the change in the transverse mechanical properties can change both the buckling mode by which failure is initiated in the fiber and also the morphological level where it is initiated. In figure-8 the change was from the shear to the extensional mode. Further studies in this area can be done by experimentally estimating the lengths of cylindrical voids and typical fibril diameters and correlating them with the compressive strength of the fiber. However at the present time there is not enough SAX data regarding the lengths of cylindical voids in rigid-rod polymer fibers to support the above conclusion [19].

4.2 BUCKLING STRENGTH AND THE MOLECULAR STRUCTURE

Considerable efforts have been directed toward improving the compressive strength of rigid-rod PBT fibers. They involved the modification of rigid-rod backbones as well as the incorporation of pendant groups. The modified rigid-rod backbones may contain bulky terphenyl units (TPBT) to disrupt the molecular packing order [20] or reactive fluorine moieties (FPBT) to form intermolecular crosslinks [21]. The pendant groups may be labile methyl groups (MPBT) with crosslinking capability [22] or hydroxyl groups (HPBT) with hydrogen bonding capability [23]. These fibers were dry-jet/wet spun and then heat treated at elevated temperatures. Their spin-draw ratio, heat treatment temperature, longitudinal tensile modulus,

tensile strength and axial compressive strength are presented in Table-4. Within each fiber, the compressive strength was found to have no relationship with the spin draw ratio, tensile modulus and tensile strength, suggesting that the compressive strength is not a function of the molecular architecture. All the modifications in the chemical structure changed the structure within the fibrils, and not the macroscopic fibril structure which was probably the structure responsible for the initiation of instability during compression loading.

Table-4: Mechanical Properties of Substituted PBT Fibers

Substituted PBT Fiber	Spin Draw Ratio	Heat Treat. Temperature (°C)	Longitudinal Modulus (GPa)	Tensile Strength (GPa)	Compressive Strength (MPa)
PBT	10-80	550-600	200-345	2.8-4.1	275-410
TPBT	2-19	500-550	190-275	1.5-2.5	275-410
MPBT	8-51	500	190-300	1.7-3.2	200-345
FPBT	10-20	420-700	165-310	1.1-3.1	310-480
HPBT	20-38	350-435	110-270	0.8-2.5	140-200

SECTION V
FIBER TORSION TEST

In the previous sections the shear modulus of the material between the fibrils in a fiber has been found to be a good measure of the fibril shear buckling load. Measurement of the torsional stiffness of the fiber is done using a torsional pendulum apparatus (figure-11) in which a disk or bar with a known moment of inertia is suspended from the fiber. Such measurements have been done in literature for textile fibers [17,18], carbon fibers [24] and for rigid-rod polymer fibers like Kevlar [6]. Ideally, these tests should be done without applying any tension on the fibers during the test. However the weight of the inertia body used in the experiment acts on the fiber and changes the measured torsional stiffness.

The torsional stiffness of a bar is theoretically found to increase with the application of a longitudinal stress [25,26]. The increase in the stiffness is negligible when the strain resulting from the applied stress is small [17,18]; however the effect becomes significant for large, finite strains [6,24]. It has been suggested in reference [6] that the amount of increase in the torsional stiffness is dependent on the degree of anisotropy of the material. Thus the relationship between the measured torsional stiffness G_m corresponding to an axial stress σ_z and the zero stress torsional modulus G has been determined to be

$$G_m = G + A\sigma_z \tag{15}$$

where A is a material dependant constant that varies from zero for isotropic materials and one for highly anisotropic materials. But this theory does not consider the effect of the initial, finite (extensional) stress on the stress-strain relationship of the material which can sometimes become significant.

5.1 ANALYSIS OF THE TORSION OF FIBERS UNDER TENSION BY THE INCREMENTAL DEFORMATION THEORY

The problem of torsion of a fiber under an initial axial stress is better analyzed using the theory of incremental deformation [26] because of the large deformations involved. According to this theory the effect of the initial stress is to change the torsional shear modulus of the fiber as shown in figure-12. A measure of this increased stiffness is the sliding shear modulus defined by

$$G'_{rz} = G_{rz} - \frac{1}{2}\sigma_z \tag{16}$$

The sliding shear modulus G_{rz} is equal to the torsional shear modulus G_{rz} of the material only

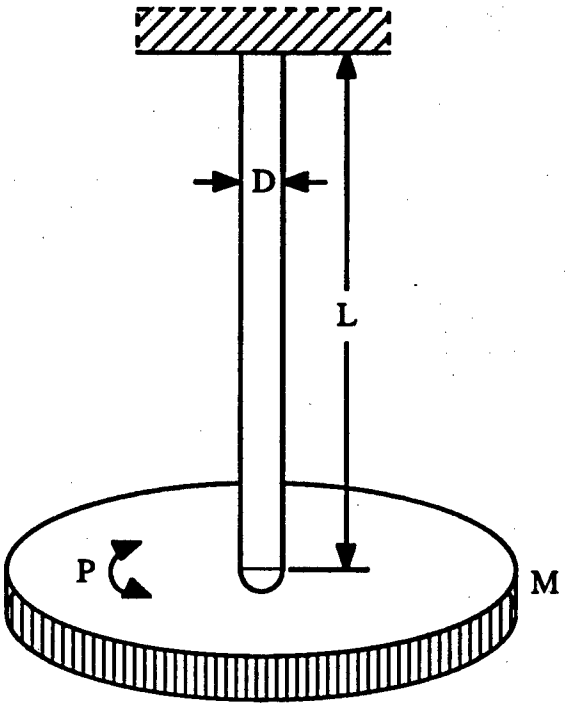

Figure-11: Torsional Pendulum

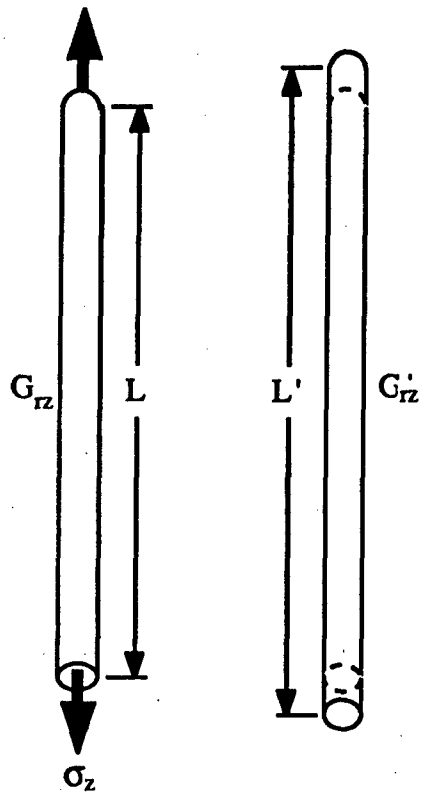

Figure-12: Axial Stress and the Sliding Modulus

when there is no applied axial stress. This relationship is true for transversely isotropic materials in which the torsional shear modulus $G_{rz}=G_{\theta z}$ is different from the inplane shear modulus $G_{r\theta}$. For isotropic materials the sliding shear modulus can be shown using this theory to be approximately the same as the shear modulus in the undeformed material. Thus

$$G'_{rz} = G \tag{16a}$$

Along with the increase in the torsional stiffness there is also an increase in the length of the fiber. If E_z is the axial modulus of the fiber then the increased length of the fiber is given by

$$L' = \left(1+\frac{\sigma_z}{E_z}\right)L \tag{17}$$

Using the incremental deformation theory the total torque per unit length acting on the cross-section of the fiber under the initial stress can similarly be determined to be [26]

$$\tau = (G'_{rz} + \sigma_z)\frac{J}{L'}\theta \tag{18}$$

where J is the polar moment of inertia of the cross-section of the fiber. Thus for the torsional pendulum we have the following equation of motion.

$$M\ddot{\theta} + \tau = 0 \tag{19}$$

Here M is the moment of inertia of the pendulum disk. Combining equations (18) and (19) and solving, the measured torsional stiffness can be written as

$$G'_m = G'_{rz} + \sigma_z = \frac{128\pi ML'}{P^2D^4} \tag{20}$$

where D is the diameter of the fiber and P is the period of oscillation.† The Poisson effect on the diameter of the fiber is neglected here because the relative change in the diameter and its fourth power is very small compared with the change in the length of the fiber. The measured torsional stiffness (G_m) as given in reference [6] is thus related to that given in equation (20) by

$$G'_m = \frac{L'}{L}G_m \tag{21}$$

5.1.1 Comparison with Experimental Results

The problem of the torsional vibration of an axially loaded fiber of length L is therefore equivalent to that of an unloaded fiber of length L' and torsional stiffness $G_{rz}'+\sigma_z$. This effect was studied by replotting the experimental data for Nylon and Kevlar 49, both anisotropic fibers, given in reference [6] taking into account the effect of the change in length due to the axial stress on the equation for the torsional pendulum. Figures 13(a) and 13(b) show that the torsional

† for the centrally bonded torsion pendulum described in reference [6] the corresponding equation is

$$G'_m = \frac{32\pi ML'}{P^2D^4} \tag{20a}$$

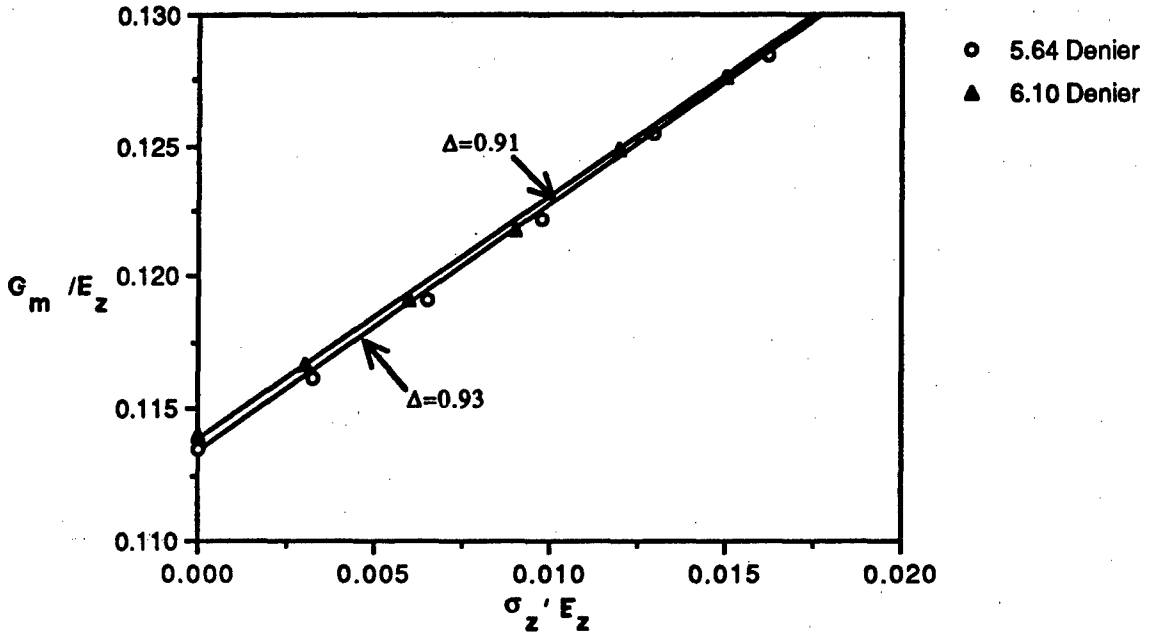

Figure-13(a): Dependence of Torsional Stiffness on Axial Stress in Nylon Fibers

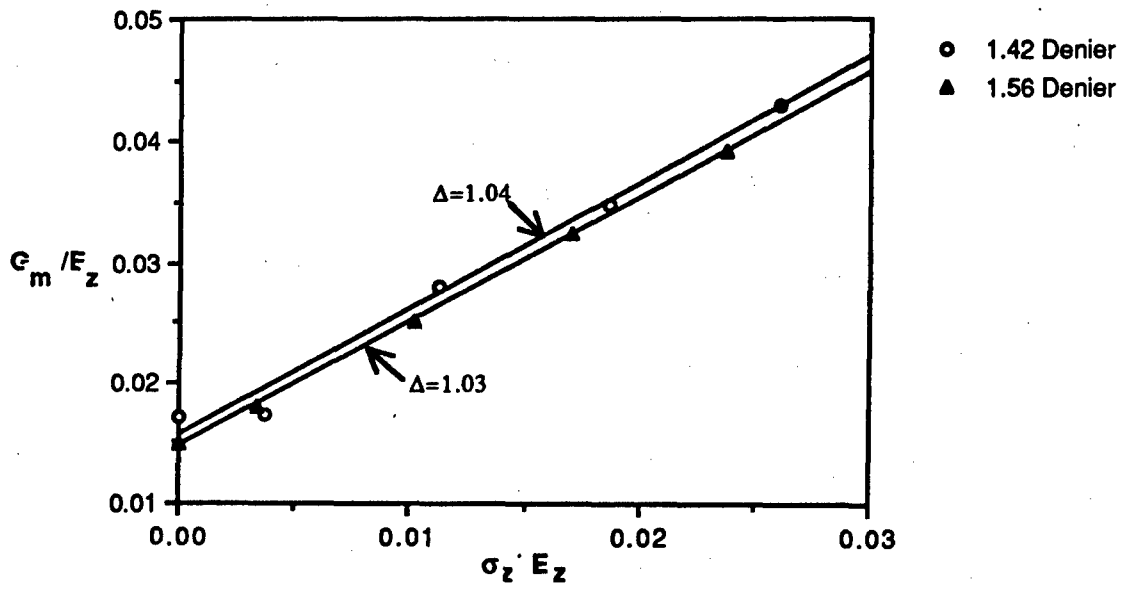

Figure-13(b): Dependence of Torsional Stiffness on Axial Stress in Kevlar 49 Fibers

stiffness $G_{rz}'+\sigma_z$ varies linearly with the axial stress σ_z with a slope of one. The experimental data for the isotropic glass fiber could not be replotted because the relative change in the period of oscillation, P, with the axial load was too small to accurately read off the plot in reference [6]. However it is expected that for all homogeneous fibers, including isotropic ones, the measured torsional stiffness will vary linearly with the axial stress with a slope of unity irrespective of the degree of its anisotropy. Torsional pendulum tests data for some transversely isotropic, homogeneous carbon fibers [24] supports this theory.

5.2 INTERPRETATION OF THE SLIDE MODULUS

If the homogeneous body under axial tension is considered to be made up of many strips parallel to its axis then the slide modulus, defined by equation (16) can be interpreted as the stiffness related to the stress parallel to the axis needed to slide one strip over the other [26]. As these strips are made smaller and smaller they can be considered to be structures analogous to the fibrils in rigid-rod polymer fibers like Kevlar and the slide modulus can be identified as the shear modulus that restricts the relative sliding between the fibrils -- the quantity G used in equation (8a).

It can be seen from figure-13 and from equation (18) that when a compressive axial stress is applied to the fiber its effective torsional stiffness G decreases and it vanishes for the condition

$$\sigma_z = - G_{rz}' \tag{22}$$

Accordingly the structure becomes unstable for any non-zero applied torque as interpreted in reference [6] for Kevlar fibers. However this condition of internal instability, identified as torsional buckling in reference [26], can occur in any transversely isotropic fiber irrespective of its microstructure as long as equation (22) is satisfied. But only for fibers with a fibrillar structure can the sliding modulus, G_{rz}', be taken to be a measure of the fibrillar shear mode buckling strength in the model described in section-II. This is because the compressive failure of the fibrillar fibers observed experimentally is caused by their internal instability as explained above.

SECTION VI
EFFECT OF PROCESSING CONDITIONS ON COMPRESSIVE STRENGTH

As discussed in the earlier sections, experimental and theoretical considerations [2,5] have shown that the fiber compressive strength most likely depends on the strength of the interaction between the fibrillar substructures within the fiber, and not on the molecular interaction between the chains. If this is true then the processing and post processing conditions that affect the magnitude of the interaction at the fibrillar level will also affect the compressive strength. On the other hand if only the transverse forces at the chain level is changed during processing then there should not be a significant change in the compressive strength. In this section some work done in this regard is discussed.

Several studies were done inhouse [21-24] to try to improve the compressive strength of PBT fibers by increasing the transverse interaction at the polymer chain level using substitution groups of varying degrees of polarity and having the capacity to crosslink. Table-4 shows that the compressive strength is not affected much by changing the substitution groups on the PBT molecule thus showing that the strength is not influenced by the interchain interaction.

6.1 EFFECT OF IRRADIATION OF THE FIBER

Work has also been done inhouse to determine the effect of degree of chain crosslinking on the compressive strength through the irradiation of pendant methyl PBT (MPBT). It is expected that during the irradiation process the radiation energy will break up some of the bonds within the molecule and induce crosslinking between adjacent polymer chains. Thus the transverse interaction within the fibrils will be affected. However the degree of entanglement between the fibrils, which contributes more to the transverse interaction at the fibrillar level, will not be affected.

As-spun methyl PBT fibers were irradiated with gamma rays upto a maximum dosage of 1 GRad. It was found (table-5) that for these fibers the change in the tensile modulus and the compressive strength with irradiation is not significant. The effect of radiation on the crosslinking between the polymer chains has been studied by measuring the change in solubility of the radiated and the un-radiated MPBT samples in methyl sulphonic acid (MSA) [27]. It can therefore be concluded that irradiation and hence the increase in transverse interaction at the chain level through crosslinking does not affect the compressive strength significantly. The fact that

Table-5: Effect of Irradiation on the Properties of Methyl PBT Fiber

	Fiber Diameter (μm)	Tensile Modulus (GPa)	Tensile Strength (GPa)	Compressive Strength (GPa)
As-spun MPBT	80-90	103	1.0-1.4	0.6-0.7
Irradiated MPBT	70-80	124	0.9-1.3	0.7-0.8

the tensile modulus did not change significantly also indicates that the degree of alignment of the chains and/or fibrils did not change much during irradiation.

6.2 EFFECT OF COLD DRAW AND HEAT TREATMENT OF THE FIBER

It has been proposed [3] that the fibrillar structure forms in the fiber during coagulation. As the fiber is rapidly cooled in the coagulant, shrinkage stresses arise in the fiber causing some of the transverse bands observed in them [2]. The effect of the residual stresses caused by the difference in the rate of heat conduction between the surface and the core of the fiber and by the lack of sufficient draw in the fiber during coagulation is that the fibrils in the fiber are not fully extended. Instead they curl up and overlap with the adjacent fibrils. Experimental evidence of the lack of order in the transverse direction comes from the fact that the as-spun fibers have lower longitudinal modulus and high tensile yield which indicates that the microstructure is not all well aligned and fully extended.

Several studies have been done to determine the effect of the degree of heat treatment on the tensile properties [2,28] and on the compressive strength [28]. It has been determined that both cold draw and heat treatment increase the longitudinal modulus and the yield strength of the fiber from its as-spun state suggesting that the microstructure (chains and fibrils) get more aligned. SAX studies [3,28] show the increase in transverse molecular order. It has also been shown that drying the fiber with an applied tension results in an increased degree of alignment in the fiber as compared to drying without tension and that more significant increase in the tensile properties occurs with heat treatment than with cold draw [28]. This has been attributed to the unraveling of the microstructure due to the applied tension and due to the evaporation of the coagulant and the solvent from the wet fiber during the heating process. Post drying heat treatment temperature does not have any significant influence on the compressive strength [28] even when the tensile modulus increases.

In house work was done on Dow PBO and DuPont PBT fibers to further study the above issue and to see if the significant increase in the tensile modulus in the heat treated fiber over the as-spun fiber is accompanied by any change in the compressive strength. The results of this work are discussed below.

Figures 14(a) and 14(b) show typical tensile stress-strain curves for the as-spun and heat treated polymeric fibers used in this study. It can be seen that for the as-spun fibers there is a small elastic region followed by a large plastic zone with a distinct yield point while the heat

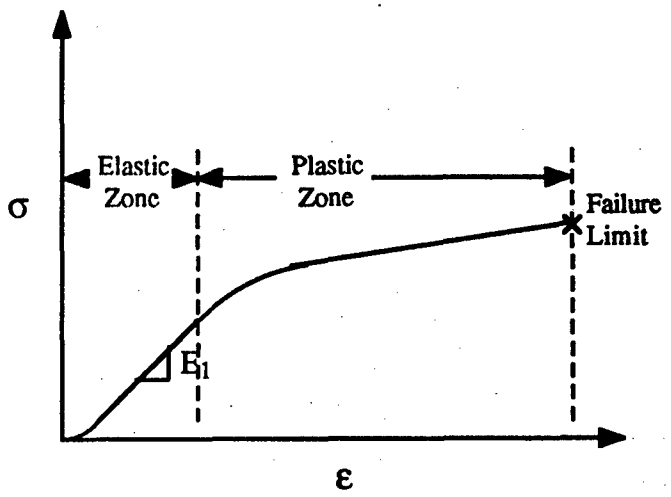

Figure-14(a): Stress-Strain Relationship in As-Spun Fiber

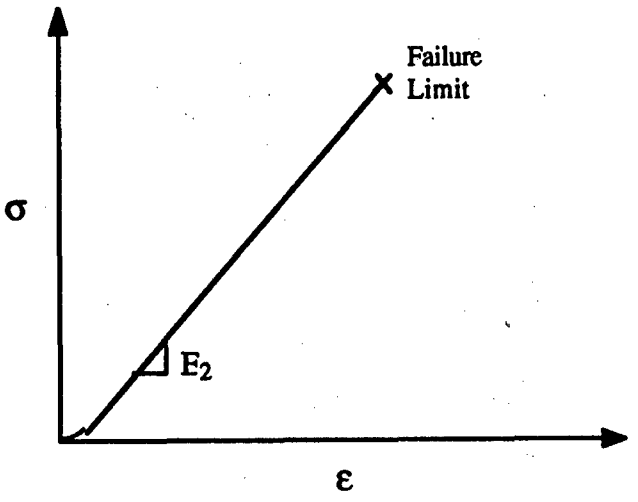

Figure-14(b): Stress-Strain Relationship in Heat Treated Fiber

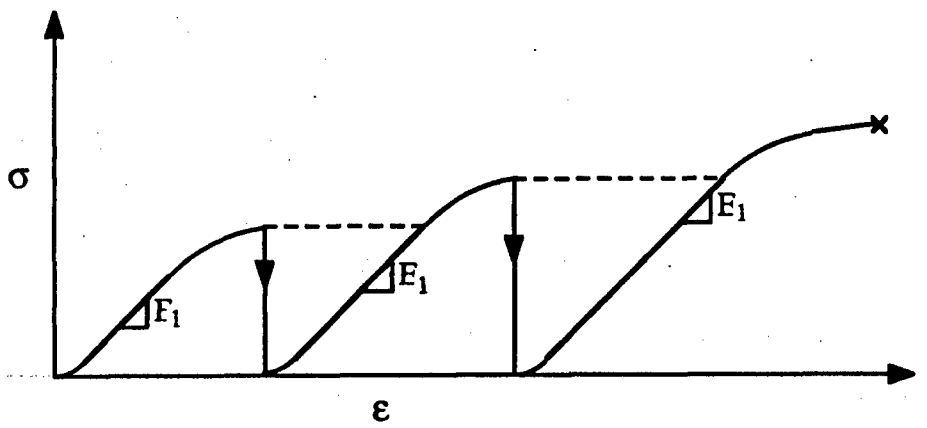

Figure-14(c): Cold Drawing of As-Spun Fiber

treated fibers behave elastically almost upto the point of failure. Thus the maximum strain to failure is much greater in the as-spun fibers while the corresponding elastic modulus is only slightly lower lower. Table-6 shows that the difference in tensile modulus between the as-spun and the heat treated fibers is not much for the PBO and the PBT fibers; this may be because the heat treatment conditions may not be completely optimized for the maximum modulus.

Another method of aligning the microstructure of the fibers is to draw it at room temperature. This is called cold draw (figure-14(c)). As the applied stress becomes greater than the yield stress of the applied fiber, it undergoes plastic deformation. On unloading the fiber and reloading it, it is found that the fiber now behaves elastically upto the point of the initial loading as shown in figure-14(c). The cold draw elastic modulus is also not much different from the as-spun elastic modulus. This shows that the linear elastic modulus is a property of the fully drawn microstructure, when the fiber does not suffer permanent deformation. Only when the applied stress becomes greater than a critical value, equal to the yield stress, the microstructure starts being extended, thus accounting for the plastic deformation of the fiber.

Table-6 also shows the effect on the recoil compressive strength. It can be seen that the there is a large drop in the compressive strength of the fiber form the as-spun state to the heat treated state. It should be mentioned here that the tensile load (corresponding to the compressive strength) used in the recoil test was less than the yield stress of the unloaded as-spun fiber i.e., the fiber was loaded within its elastic region and therefore did not suffer permanent deformation. In the case of the cold drawn PBO fiber too the recoil compressive stress decreases from the as-spun value and approaches the heat treated value. The value of the cold draw stress used was about 1.7 GPa which was greater than the yield stress of 0.5 GPa for the as-spun PBO fiber. Thus corresponding to an increase in the lateral order of the microstructure of the fiber either due to heat treatment or due to cold draw there is a decrease in the compressive strength. The above observations support the earlier statement that when the fibrils are all better aligned along the fiber axis there is less transverse interaction (figure-15) and this appears to lower the compressive strength of the fiber.

More tests with better quality fibers have to be done before any final conclusion can be made. The as-spun PBO and PBT fibers used in this experiment had kink bands present in them; some of which disappeared under tension. However they could have affected the compressive strength values by acting as precursors for the kink bands observed during the recoil test and may be the reason for some of the scatter observed in the compressive strength data, especially for the PBT fibers.

Table-6: Effect of Heat Treatment on Mechanical Properties

Fiber	Type	Fiber Diameter (μm)	Tensile Modulus (GPa)	Tensile Strength (GPa)	Compressive Strength (GPa)
PBO	As-spun	50-55	147	2.0-2.6	0.43
	Cold Drawn	50-55			0.28
	Heat Treated	50-55	164	1.0-1.5	0.27
PBT	As-Spun	20	171	1.6-1.7	0.5-0.7
	Heat Treated	17-19	256	2.0-2.5	0.28

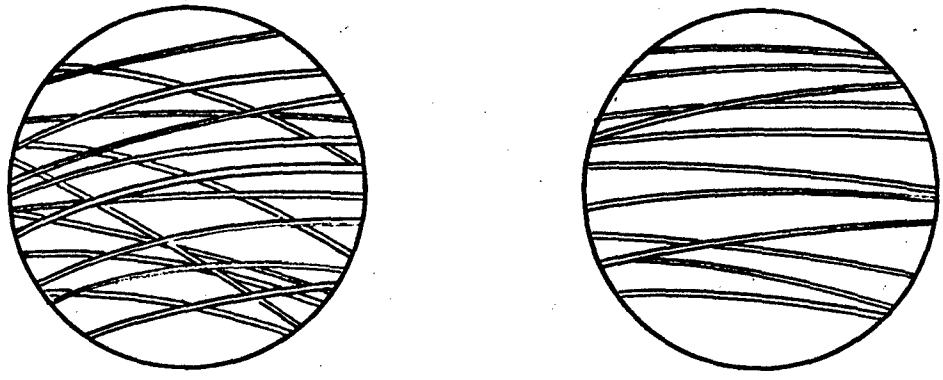

(a) As-Spun Fiber (b) Heat Treated Fiber

Figure-15: Alignment of Fibrils in Fiber

SECTION VII
CONCLUSIONS

Various mechanical models describing the buckling of a single column and a bundle of columns are reviewed and the relationship between these models and the buckling of a polymeric fiber with substructures (fibril, microfibril and individual chain) are discussed. Numerical results indicate that the structural element that has the lowest critical buckling strength will initiate the compressive failure of the fiber. The failure mode and the critical strength when buckling initiates in the fiber may not always correspond to the shear mode of buckling instead it is dependent on the element geometry, and the strength of the interaction with the neighbors. In previous analysis in the literature, the equations were applied to the molecular chain level. This study shows that the analysis is more appropriate at the fibril level (diameter of 0.1 μm).

Results from the studies of rigid-rod polymer fibers with modified molecular structures are discussed. Though substitution groups with varying degrees of polarity were used there was no significant difference in the compressive strengths of the fibers indicating that the interactions between the polymer chains within the fibrils do not affect the mechanism of compressive strength. This supports the idea mentioned in this report that it is more relevant to apply the buckling equations at the level of the fibrils rather than at the chain level.

The mechanics of the fiber torsion test has been re-assessed from the point of view of the incremental deformation theory which, unlike the linear elastic theory, considers the effect of the axial stress on the stress-strain relationship of the anisotropic fiber. According to this theory the torsional modulus measured in the fiber torsion experiment must be linearly related to the axial stress for all homogeneous materials unlike as reported in earlier work. Experimental results from this earlier work has been shown to be in support of this conclusion. The incremental deformation theory has also been used to explain how the measured torsional stiffness is actually a measure of the shear modulus that describes the sliding between the microstructure in a fiber with a fibrillar structure. The condition of torsional instability when the measured torsional stiffness of the fiber vanishes occurs when the applied axial compressive load is equal to the sliding shear modulus of the microstructure in the fiber. According to the buckling equations described in section III this corresponds to the compressive strength of a fiber in which the failure initiates by the shear mode buckling of the microstructure.

Finally the results of some preliminary cold draw experiments on as-spun and heat treated fibers have been reported. Some results seem to indicate a drastic descrease in the compressive

strength of the fiber, upto 50%, with cold drawing and heat treatment. If this is true this may be identified with the decrease in the lateral interactions between the fibrils that accompanies the axial ordering of the microstructure in the fiber during the drawing and the heat treating processes as suggested by the buckling theories discussed in this report. However more work needs to be done before any definite conclusions can be drawn.

REFERENCES

1. Kumar, S., 'Structure and Properties of High Performance Polymeric and Carbon Fibers -- An Overview', *SAMPE Quarterly*, 3 (1989).
2. Allen, S. R., 'Mechanical and Morphological Correlations in Poly (p-Phenylene Benzobisthiazole) Fibers', Air Force Technical Report, AFWAL-TR-83-4065 (1983).
3. Cohen, Y., and Thomas, E. L., 'Fibrillar Network of a Rigid Rod Polymer. 1. Visualization by Electron Microscopy', *Macromol.*, 21, 433 (1988).
4. Sawyer, L. C., and Jaffe, M., 'The Structure of Thermotropic Copolysters', *J. Mater. Sci.*, 21, 1897 (1986).
5. DeTeresa, S. J., 'The Axial Compressive Strength of High-Performance Polymer Fibers', Air Force Technical Report, AFWAL-TR-85-4013 (1985).
6. Allen, S. R., 'Stress-Coupling Phenomena in Anisotropic Fibers', *Polymer*, 29, 1091 (1988).
7. Dobb, M. G., Johnson, D. J., and Saville, B. P., Compressional Behavior of Kevlar Fibers', *Polymers*, 22, 960 (1981).
8. Lee, R. J., 'Compression Strength of Aligned Carbon Fiber-Reinforced Thermoplastic Laminates', *Composites*, 18(1), 35 (1987).
9. Timoshenko, S. P., and Gere, J. M., Theory of Elastic Stability, 2d. ed., McGraw Hill Book Co., New York (1961).
10. Van der Zwaag, S., et. al., 'Kinkband Formation in Aramid Fibers', Rolduc Polymer Meeting, Rolduc, Netherlands (1988).
11. Wilfong, R. E., and Zimmerman, J., 'Strength and Durability Characteristics of Kevlar Aramid Fiber', *J. Appl. Polym. Sci.: Appl. Polym. Symp.*, 31, 1 (1977).
12. Rosen, B. W., 'Mechanics of Composite Strengthening', Fiber Composite Materials, American Society for Metals Seminar (1964).
13. Greszczuk, L. B., 'Microbuckling Failure of Circular Fiber-Reinforced Composites', *AIAA Journal*, 13(10), 1311 (1975).
14. ASTM D3379-75e, 'Standard Test Method for Tensile Strength and Young's Modulus of High-Modulus Single-Filament Materials', ASTM, Philadelphia (1975).
15. Phoenix, S. L., and Skelton, J., 'Transverse Compressive Moduli and Yield Behavior of Some Orthotropic, High-Modulus Filaments', *Tex. Res. J.*, 44(12), 934 (1974).
16. Hadley, D. W., Pinnock, P. R., and Ward, I. M., 'Anisotropy in Oriented Fibers from Synthetic Polymers', *J. Matér. Sci.*, 4, 152 (1969).
17. Meredith, R., 'The Torsional Rigidity of Textile Fibers', *J. Text. Inst.*, 45(7), 489 (1954).

18. Wakelin, J. H., et. al., 'Vibroscope Measurements of the Elastic Moduli of Nylon 66 and Dacron Filaments of Various Draw Ratios', *J. Appl. Phy.*, 26(7), 786 (1955).
19. Bai, S. J., Private Communication.
20. Wang, C. S., et. al., 'Disruptive Packing Order via Bulky Benzobisthiazole Rigid-Rod Polymers', ACS PMSE Proceedings, American Chemical Society, Washington DC, 60, 767 (1989).
21. Chuah, H. H., et. al., 'Crosslinked Benzobisthiazole Rigid-Rod Copolymers via Labile Methyl Groups', ACS PMSE Proceedings, American Chemical Society, Washington DC, 60, 517 (1989).
22. Bhattacharya, S., et. al., 'Rigid-Rod Benzobisthiazole Polymers with Reactive Fluorine Moieties: II. Fiber Processing, Properties and Morphology', ACS PMSE Proceedings, American Chemical Society, Washington DC, 60, 512 (1989).
23. Dang, T. D., et. al., 'Pseudo-Ladder Structure via Dihydroxy Pendant Benzobisthiazole Rigid-Rod Polymers', ACS PMSE Proceedings, American Chemical Society, Washington DC, 60, 424 (1989).
24. Seshadri, S., 'Dynamic Torsional Behavior of Carbon Fibers', PhD. Dissertation, Univ. of Washington (1979).
25. Timoshenko, S. P., Strength of Materials, vol. II, 3d ed., McGraw Hill Book Co., New York (1958).
26. Biot, M. A., Mechanics of Incremental Deformations, John Wiley & Sons, Inc., New York (1965).
27. Wang, C. S., Private Communication.
28. Pottick, L. A., 'The Influence of Drying on the Structures and Mechanics of Poly (p-Phenylene Benzobisthiazole) Fibers', Air Force Technical Report, AFWAL-TR-86-4055 (1986).
29. UDRI, 'Exploratory Development on Polymeric Materials for Advanced Aircraft and Aerospace Vehicles', Air Force Technical Report, AFWAL-TR-88-4084, p. 245-256, 269-271 (1988).
30. Minter, J. R., et. al., 'Microstructural Study of As-Extruded and Heat Treated Ribbons of PBZT', *J. Mater. Sci.*, 16, 3303 (1981).
31. Minter, J. R., 'Structural Investigations of Fibers and Films of PBT', Air Force Technical Report, AFWAL-TR-,
32. Cohen, Y., and Thomas, E. L., 'Structure Formation During Spinning of PBT Fiber', *Polym. Eng. & Sci.*, 25(17), 1093 (1985).
33. Cohen, Y., and Thomas, E. L., 'Fibrillar Network of a Rigid Rod Polymer. 2. SAX Scattering', *Macromol.*, 21, 436 (1988).

34. Cohen, et. al., 'Structure Formation and Phase Transformations in Solutions of a Rigid Polymer', Thermoreversibile Gelations, Paul Russo ed., ACS Symposium Series, July (1986).
35. Pottick, L. A., and Farris, R. J., 'The Effect of Tension During Drying on the Structure and Mechanics of PBZT Fibers', *Polym. Eng. & Sci.*, 25(5), 284 (1985).

APPENDIX
LITERATURE REVIEW OF MORPHOLOGY OF PBT AS RELATED TO ITS COMPRESSIVE STRENGTH

Observations	Reference
1. Core-sheath structure of the fiber	Kumar[29]
2. Fibrillar structure of the fiber	Allen[2], Minter[30,31], Cohen[3, 32-34], Satish[29]
3. Fibrillar dimensions and structure:	
• Width ~ 70Å; Ribbon shaped fibril	Allen[2]
• Diameter ~ 80-100Å; Cylindrical fibril	Cohen[32]
• Average diameter by SAX ~ 71Å; Irregular shaped cross-section	Cohen[33]
• Length of microfibril ~ 100s to 1000s Å	Cohen[3]
4. Local ordered region in the fiber (within the fibril):	
• In as-spun fibers ~ 20Å, 20 chains	Allen[2]
• In heat treated fibers ~ 120Å, 200 chains	Allen[2]
• As-spun fiber ~ 20Å; heat treated fiber ~ 100Å	Minter[30,31]
• Length parallel to the fiber axis ~ 150Å (Maximum length observed ~ 400Å)	Minter[31]
5. Voids in and between the fibrils:	
• Voids within the fiber (PBT/MSA has more voids than PBT/PPA)	Allen[2]
• Density of microfibrils < Density of PBT crystal	Cohen[32]
6. Formation of microfibrils:	
• The microfibrils are formed and the dimensions set during the coagulation process and are not affected by heat treatment.	Cohen[3]
• Microfibrils formed by the high nucleation density during rapid coagulation in water. Low nucleation density caused by slow coagulation by moisture results in a lamellar morphology.	Cohen[34]
7. Buckling of fiber/fibrils:	
• Evidence that buckling of fiber implies the buckling of the fibrils / microfibrils.	Cohen[3]

- In as-spun PBT fiber, residual compressive stress in the outer surface of the fiber causes this region to buckle. Allen[2]
- Strain hardening behavior in as-spun PBT is caused by the straightening of the buckled elements due to relief of the residual stresses. Allen[2]

8. Effect of heat treatment:
   - The lateral molecular order and the degree of axial orientation increases with the heat treatment temperature. Allen[2]
   - Annealing under slight tension increases the degree of lateral molecular order, but keeps the molecular orientation along the axis constant (evidence from WAXD, SAED). Minter[30]
   - Applying tension during drying increases the tensile properties by straightening the microfibrillar network and decreasing the magnitude of the axial compressive shrinkage stress. WAX data shows that tensioning the fiber in the wet state is better than tensioning in the dry (as-spun) state. Pottick[35]

☆U.S.Government Printing Office: 1990—748-056/24307